https://doi.org/10.5194/egusphere-2026-826
Preprint. Discussion started: 20 May 2026

High-Resolution Modelling of Landfast Ice Formation and Midseason Breakout on the Siberian Shelf

Xuezhi Bai[1], Ziqing Dong[1], Kaiwen Wang[1], Xian Jiang[1] and Wenjing Zhang[2]

[1]College of Oceanography, Hohai University, Nanjing, 210098, China
[2]College of Meteorology and Oceanography, National University of Defense Technology, Changsha, 410073, China

Correspondence to: Xuezhi Bai (xuezhi.bai@hhu.edu.cn) and Wenjing Zhang (zhangwenjing21@nudt.edu.cn)

Abstract. Substantial amounts of landfast ice form over the Siberia shelf seas during winter. Under certain conditions, midseason break out may occur, affecting local ecology and human activities. This study employed a 2 km resolution coupled ocean-ice model incorporating a basal stress parameterization to simulate landfast ice in the Siberian Seas. The high- resolution model yields realistic simulations of landfast ice distribution in the Siberian Seas. The contribution of the grounding mechanism to landfast ice stability varies regionally and depends strongly on local geography. Grounded fast ice accounts for 56% of the total simulated landfast ice on the Siberia shelf, with the East Siberia Sea having the largest proportion (70%), followed by the Laptev Sea (54%) and the Kara Sea (41%). The simulated midseason breakout events primarily occurred along the outer edge of the landfast ice in the East Siberia Sea, where the basal stress was ineffective. Further analysis reveals that all the midseason breakouts were associated with the passage of cyclones, whose offshore winds fractured the landfast ice into floating ice.

https://doi.org/10.5194/egusphere-2026-826
Preprint. Discussion started: 20 May 2026

1 Introduction

Landfast ice, defined as stationary sea ice attached to the coast or seafloor, is an important seasonal feature of the Arctic coastal zone. Its extent is strongly influenced by local topography and bathymetry, with the fast ice edge typically located within the 10–25 m depth range on average (Divine et al., 2004; Mahoney et al., 2007a, b). Landfast ice plays multiple roles: it mitigates coastal erosion, serves as a platform for transportation and offshore exploration, and provides a habitat for marine organisms (Eicken et al., 2009; Hughes et al., 2011; Radosavljevic et. al, 2016). Conversely, it also significantly impedes navigation, posing a major challenge to the utilization of the Northeast Passage. Furthermore, the fast ice edge defines the location of polynyas and thereby controls local ocean processes governed by sea ice formation and brine rejection, as well as atmospheric mesoscale motion (Maqueda et al., 2004).

Over one-third of the Arctic's landfast ice is located in the Siberian Seas—the Kara, Laptev, and East Siberian Seas—where its winter edge can extend 300–500 km from the coast (Yu et al., 2014; Selyuzhenok et al., 2017; Zhai et al., 2021). The irregular coastline, shallow waters, and archipelagos create favorable conditions for landfast ice development. The mechanisms that stabilize fast ice vary across the Siberian shelf, largely influenced by local geography. In the shallow Laptev and East Siberian Seas, grounding—where pressure ridges freeze to the seafloor—is a dominant stabilizing process (Haas et al., 2005; Selyuzhenok et al., 2017; Lemieux et al., 2018). In the deeper Kara Sea, the grounding mechanism is less effective, and stabilization relies more on island chains acting as natural anchoring points (Divine et al., 2005; Olason, 2016). Additionally, the tensile strength of the ice itself plays a crucial role in sustaining extensive landfast ice cover (Tremblay and Hakakian, 2006).

Landfast ice is usually stable during wintertime; however, under certain circumstances, portions of landfast ice may occasionally detach from the coast or the edge of the landfast ice, an event referred to as a midseason breakout (Gearheard et al., 2006). In recent decades, Arctic and subarctic landfast ice has been increasingly unstable and prone to breakouts (Gearheard et al., 2006; Huntington et al., 2013; Meier et al., 2006). These midseason breakouts disrupt the essential provisions and ecosystem services of landfast ice and introduce challenges and hazards. They usually occur when the grounded ridges fail or become ungrounded, generally caused by strong atmospheric and oceanic stresses without the influence of thermodynamic melting (Jones et al., 2016; Mahoney et al., 2007a, b). Using either in-site or satellite observations, midseason break outs along the northern coast of Alaska, Chukchi Sea and northern Bering Sea have been studied (Jones et al., 2016; Borgardus et al. , 2020 and Jensen et al., 2023).

Numerical models are powerful tools for simulating, predicting and understanding the mechanism and variability of landfast ice. Substantial efforts have been made to incorporate various stabilizing mechanisms into sea-ice models over the past decade. Early approaches focused on adjusting internal sea-ice strength parameters within viscous-plastic rheology to represent landfast ice (Beatty and Holland, 2010; Olason, 2012; Itkin et al., 2015). To better capture conditions in shallow waters, Lemieux et al. (2015) parameterized the grounding of ice keels by introducing a basal drag term dependent on topography and ice thickness. This framework was later refined by Lemieux et al. (2016), who combined tensile strength with basal stress parameterization

https://doi.org/10.5194/egusphere-2026-826
Preprint. Discussion started: 20 May 2026

to improve simulations in the Kara Sea. More recently, Liu et al. (2022) proposed a lateral drag parameterization to simulate the pinning effect of coastlines and islands, enabling sea ice to remain fast nearshore.

While Pan-Arctic large-scale models incorporating various parameterizations can produce broadly realistic simulations of Arctic landfast ice and are very usefully for basin scale and climate studies (Itkin et al., 2015; Lemieux et al., 2015, 2016; Olason, 2016; Liu et al., 2022), their coarse resolution—typically ranging from 10 km to 36 km—often fails to adequately represent small islands and shallow topographic features. As a result, those models rely on the parametrizations to capture subscale information to reproduce landfast ice, often leading to unrealistic simulation of landfast ice at regional scales.

Recognizing the critical role of resolution in accurately simulating landfast ice, this study establishes a 2 km high-resolution coupled ocean-ice regional model based on the MITgcm to study landfast ice in the Kara, Laptev, and East Siberian Seas. Given the extensive shallow waters in this region, the model incorporates the basal stress parameterization developed by Lemieux et al. (2015). In this study, we evaluated the simulated landfast ice in terms of its spatial and temporal variability against the ice charts from the U.S. National Ice Centre (NIC), quantified the relative contributions of the grounding and other stabilizing mechanisms to the total landfast ice cover and their regional variability. We also studied midseason breakout events in the East Siberia Sea and their driving mechanisms.

2 Data and methods

2.1 Data

The weekly/biweekly Arctic Sea Ice Charts from NIC are used to validate the simulation. The ice charts are in Equal Area Scalable Earth Grid (EASE-Grid 2.0) format at 10-km resolution, spanning 2003 to present. These charts are primarily intended to assist operations in ice-covered waters. The early charts were available only in paper format, whereas later charts also come in digital format. Mapped with polygons containing information on sea ice concentration and ice types, a chart identifies areas of landfast ice and their boundaries (Yu et al. 2014). The Japanese 55-year Reanalysis (JRA-55; Kobayashi et al., 2015) 6-hourly dataset is used to drive the regional coupled ice-ocean model and investigate the atmospheric conditions during midseason breakout events of landfast ice. JRA-55 data have a spatial resolution of 0.25°×0.25°.

2.2 Basal stress parameterization

Considering the significant extent of shallow water in the Siberian Seas, the model adopts the basal stress parameterization developed by Lemieux et al. (2015) to simulate the landfast ice. A basal stress term $\boldsymbol{\tau_b}$ is defined and added it to the right side of the momentum equation. The modified momentum equation for sea ice is:

$$m\frac{D\boldsymbol{u}}{Dt} = -mf\boldsymbol{k}\times\boldsymbol{u} + \boldsymbol{\tau_a} + \boldsymbol{\tau_o} + \boldsymbol{\tau_b} - mg\nabla H + \boldsymbol{F}\,, \quad (1)$$

https://doi.org/10.5194/egusphere-2026-826
Preprint. Discussion started: 20 May 2026

where m is the mass of snow and ice in one unit area, $\boldsymbol{u} = u\boldsymbol{i} + v\boldsymbol{j}$ is the horizontal velocity vectors of ice, $\frac{D}{Dt}$ is the total derivative, f is the Coriolis parameter, $\boldsymbol{i}$, $\boldsymbol{j}$, $\boldsymbol{k}$ is the unit vector in the direction of x, y, z axis in Cartesian coordinate system, $\boldsymbol{\tau_a} = \tau_{ax}\boldsymbol{i} + \tau_{ay}\boldsymbol{j}$ is the wind-ice stress and $\boldsymbol{\tau_o} = \tau_{ox}\boldsymbol{i} + \tau_{oy}\boldsymbol{j}$ is the ocean-ice stress, $\boldsymbol{\tau_o} = \tau_{ox}\boldsymbol{i} + \tau_{oy}\boldsymbol{j}$ is the basal stress, g is the ∇H is the gradient of the sea surface dynamic height, $\boldsymbol{F} = \nabla \cdot \sigma$ is the divergence of the internal ice stress tensor σ_{ij}.

According to Lemieux et al. (2015), the basal stress $\boldsymbol{\tau_b}$ is given by:

$$\boldsymbol{\tau_b} = \begin{cases} 0 & \text{if } \mathrm{h} \le \mathrm{h_c}, \\ \mathrm{k_2}\left(\frac{-\mathbf{u}}{|\mathbf{u}|+\mathrm{u_0}}\right)(\mathrm{h}-\mathrm{h_c})\exp^{-\mathrm{C_b}(1-\mathrm{A})} & \text{if } \mathrm{h} > \mathrm{h_c}, \end{cases} \quad (2)$$

Where A is the sea ice concentration, $|\mathbf{u}| = \sqrt{u^2 + v^2}$, $\mathrm{u_0}$ is a small velocity parameter set to $5\times10^{-5}\mathrm{m\ s^{-1}}$ in our simulations, h is the thickness of the sea ice in a unit, $h_c = A\,h_w/k_1$ is the critical mean thickness where h_w is the water depth, $\mathrm{C_b}$ is a constant set to 20, $\mathrm{k_1}$ and $\mathrm{k_2}$ are adjustable parameters, are set to 7 and 15 N $\mathrm{m^{-3}}$, respectively.

2.3 Model description and implement

The model used is a regional coupled ice-ocean model based on the Massachusetts Institute of Technology Ocean Circulation Model (MITgcm, Marshall et al., 1997). The sea ice model is based on a variant of the viscous-plastic (VP) dynamic thermodynamics (Zhang & Hibler, 1997) described by Losch et al. (2010), i.e., elastic-viscous-plastic rheology, with an elliptic yield-curve scheme with normal flow rule, using the solver introduced by Hunke and Dukowicz (1997). Most of the parameters for this regional model followed the 4 km Arctic model configuration given by Nguyen et al. (2012).

The model domain (40°-200°E, 66°-82°N), shown in Figure 1, covers the Kara Sea, Laptev Sea, East Siberian Sea, Chukchi Sea, and parts of Barents Seas, with the western boundary located in the Barents Sea, and the eastern boundary near the Beaufort Sea. The horizontal grid has a longitudinal resolution of 0.08° and a latitudinal resolution of 0.018° (~2 km) comprising 1,876×888 grid cells. The model has 71 unevenly distributed vertical layers with high surface resolution and low deep-layer resolution, consistent with the vertical layer settings of Leng et al. (2021). The model uses IBCAO_V3_30arcsec_RR bathymetry data with a resolution of 30×30 arcsec, which is a reset version of the IBCAO V3 500m resolution data and is more suitable for polar regions (Jakobsson et al., 2012). We interpolated this bathymetric data onto the 2 km grid, smoothed it, and set the minimum water depth to 10 meters.

The initial ocean conditions, including temperature and salinity, are from the Estimating the Circulation and Climate of the Ocean, Phase II (ECCO2) solution (Menemenlis et al., 2008), and the initial sea ice conditions, including sea ice concentration and sea ice thickness, are from National Snow and Ice Data Center (NSIDC) (Fetterer et al., 2015; Key et al., 2019). The lateral boundary conditions are ocean temperature, salinity, velocity, sea ice concentration, sea ice thickness and sea ice drift averaged over every three days. Sea ice motion data are from NSIDC (Tschudi et al., 2019). Atmospheric forcing is from the Japanese 55-year Reanalysis 6-hourly dataset (JRA-55; Kobayashi et al., 2015), including 2m air temperature, 2m specific humidity, 10m winds, sea level pressure, downward shortwave and longwave radiation, and precipitation. Additionally, in the Siberia

https://doi.org/10.5194/egusphere-2026-826
Preprint. Discussion started: 20 May 2026

Seas, rive runoff is important for maintaining the stratification and likely influence landfast ice formation (Eicken et al., 2005). The climatological monthly mean rive runoff and temperature used in the model are from the Arctic River Discharge and Temperature (ARDAT) dataset (Whitefield et al., 2014).

We conducted two three-year simulations from September 1, 2012 to September 1, 2015: a control run excluding basal stress and a BD run that included it. The model was initialized from the nearly ice-free conditions of September 1, 2012. Using daily output, landfast ice is identified in grid cells where the biweekly average ice speed is smaller than 0.5 mm/s and the sea ice concentration exceeds 0.8. This two-week averaging window aligns the analysis with the temporal resolution of the National Ice Center (NIC) ice charts used for comparison.

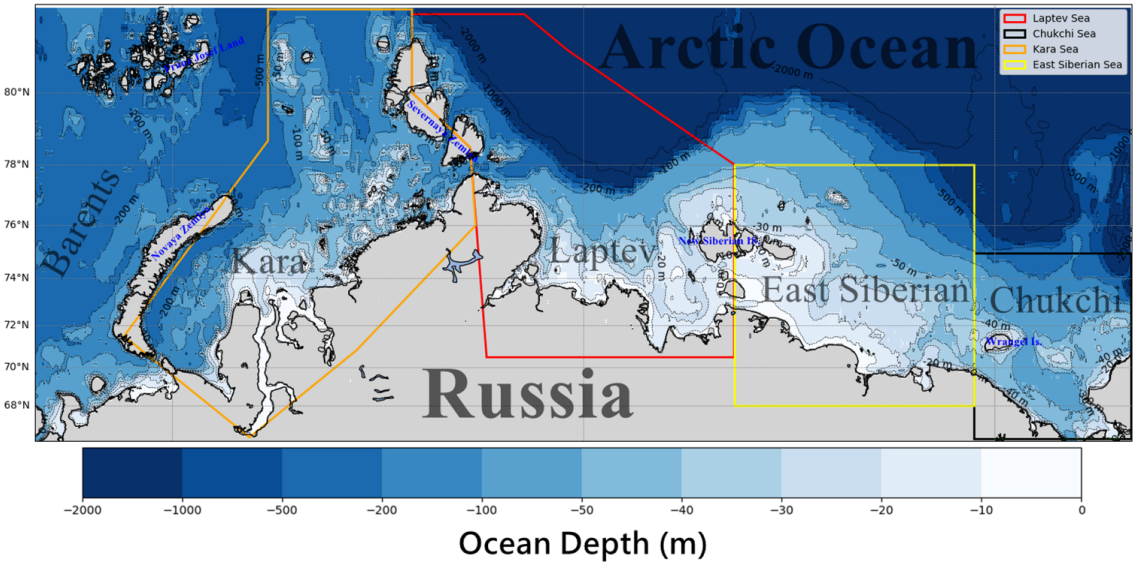

Figure 1: Model domain (40-200°E, 66-82°N) and bathymetry (in meters). Colored boxes denote the major shelf seas: the Kara Sea (orange), Laptev Sea (red), East Siberian Sea (yellow), and Chukchi Sea (black). Land areas are shown in grey.

3 Results

3.1 Spatial distribution of landfast ice

Figure 2 presents snapshots of landfast ice distribution from both NIC observations and model simulations during the winter of 2013–2014. The BD experiment, which incorporates a basal stress parameterization, yields highly realistic simulations of landfast ice and offshore flaw polynyas in the Siberian Seas. In contrast, the control run (CTRL) substantially underestimates the landfast ice extent and produces unrealistic nearshore flaw polynyas. In the BD simulation, landfast ice begins to form along the coast in November and gradually expands offshore, eventually covering nearly the entire shallow shelf as air

https://doi.org/10.5194/egusphere-2026-826
Preprint. Discussion started: 20 May 2026

temperatures decline. The Laptev and East Siberian Seas exhibit more extensive landfast ice coverage than the Kara Sea, with the broadest extent occurring in the southeastern Laptev Sea.

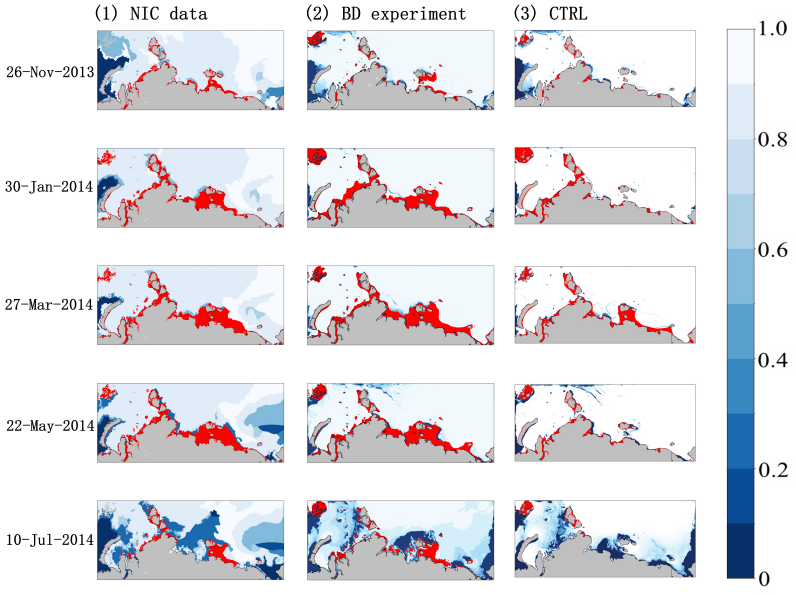

Figure 2: Sea ice concentration and landfast ice (red shade) on typical days during winter 2013-2014 for (left) NIC data, (middle) BD and (right) control run. The landfast ice is marked with red shade.

To evaluate the spatial distribution of landfast ice, we computed its occurrence frequency from January to May following the method of Yu et al. (2014), where a higher frequency indicates greater persistence. As illustrated in Fig. 3, the CTRL run systematically underestimates landfast ice throughout the region, whereas the BD simulation aligns more closely with the observations. In the BD experiment, landfast ice with an occurrence frequency exceeding 70% is predominantly located over shallow inner shelves and around island chains, particularly in the vicinity of the New Siberian Islands. The frequency decreases offshore with increasing water depth, a pattern generally consistent with NIC observations (Fig 3a).

The frequency difference between BD experiment and the observations (Fig. 3d) shows that BD experiment overestimates landfast ice in the Laptev and East Siberian Seas but underestimates it in the Kara Sea. Pronounced positive deviations are found in the southwestern Laptev Sea, north of the New Siberian Islands, and near the mouth of the Ob River—areas characterized by inlets and islands. Conversely, large negative deviations occur primarily southwest of Severnaya Zemlya in the eastern Kara Sea, where the water depth is too great for ice keels to ground.

https://doi.org/10.5194/egusphere-2026-826
Preprint. Discussion started: 20 May 2026

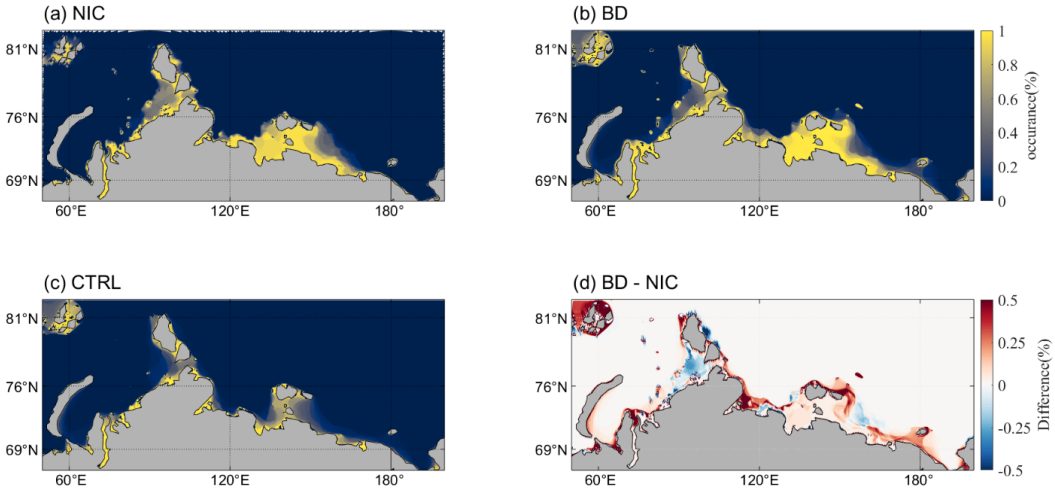

Fig. 3 Wintertime (January–May) landfast ice occurrence for the years 2013, 2014, and 2015. (a) NIC observations, (b) BD experiment with basal stress, (c) control run without basal stress, (d) differences between BD and NIC observations

3.2 Seasonal cycle of landfast ice extent

Figure 4 illustrates the areal extent of landfast ice across the entire domain and the three individual seas from the NIC data, BD and CTRL runs over the three-year period. The total landfast ice coverage from the BD experiment is further delineated into grounded and ungrounded components, which are also shown in Fig. 4. Grounded landfast ice is identified separately from the total based on the activation of basal stress, while the ungrounded portion comprises the remainder of the simulated landfast ice.

As shown in Fig. 4, the BD experiment successfully captures the seasonal cycle and magnitude of the extent of landfast ice in the Siberia Seas. However, both the CTRL and BD experiment simulates a shorter landfast ice season compared to the NIC data, characterized by a later onset across the entire study region. This discrepancy, which has also been reported in other modelling studies, may be attributed in part to inaccuracies in the representation of sea ice thermodynamics (Lemieux et al., 2016). Nevertheless, the BD experiment reproduces the rapid seasonal breakup of landfast ice reasonably well.

In addition to seasonal changes, landfast ice extent shows remarkable short-term variability, likely attributable to synoptic scale atmospheric variations. The Kara Sea experiences the most significant short-term fluctuations, with the East Siberian and Laptev Seas following. This pattern occurs because landfast ice in the Kara and East Siberian Seas is more responsive to atmospheric forcing than that in the Laptev Sea. The primary reason lies in their contrasting geographies: the greater depth of the Kara Sea, the direct open-ocean connection of the East Siberian Sea, and the Laptev Sea's sheltered configuration—featuring a complex, indented southern shore and protective archipelagos to the east and west.

https://doi.org/10.5194/egusphere-2026-826
Preprint. Discussion started: 20 May 2026

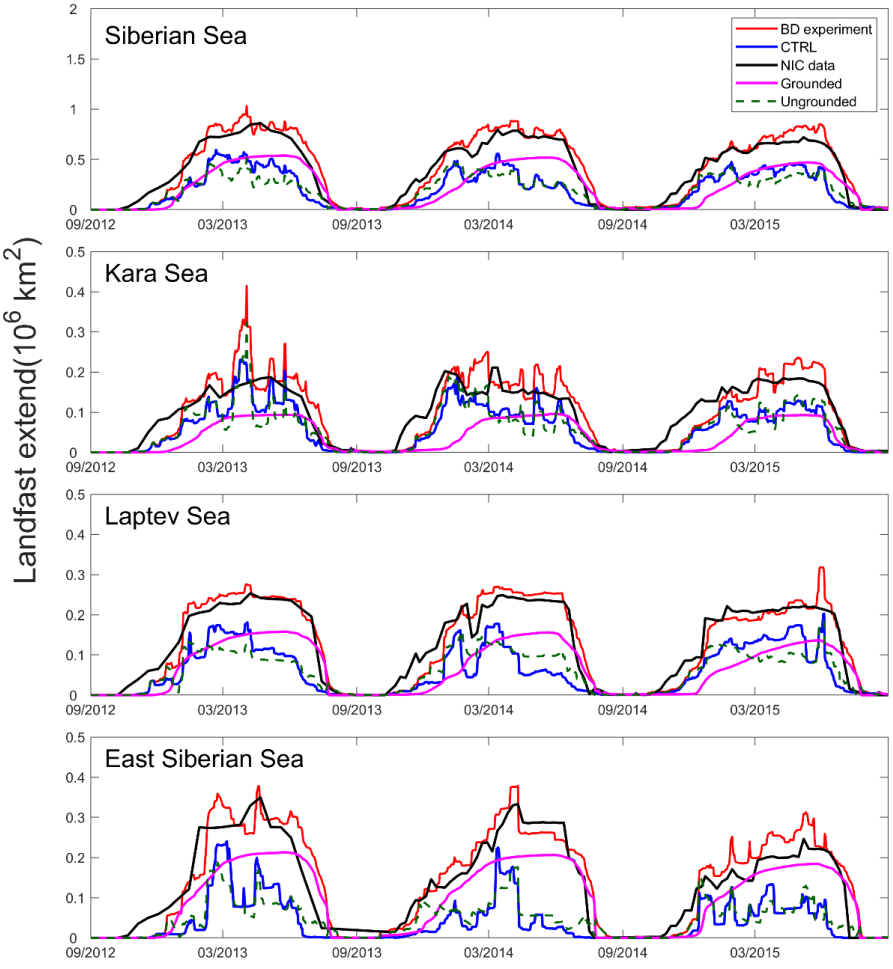

165 **Figure 4: Time series of landfast ice areal extent from September 2012 to September 2015 in the Siberian Seas for (a) the entire study domain, (b) the Kara Sea, (c) the Laptev Sea, and (d) the East Siberian Sea. Results from the BD experiment (red line) and the control run (blue line) are compared with the U.S. National Ice Center (NIC) observations (black line). The contributions of grounded (magenta) and ungrounded (green) ice to the simulated totals are also shown.**

The short-term fluctuations arise primarily from ungrounded landfast ice (blue line, Fig. 4), which exhibits variability similar 170 to the CTRL run (green line, Fig. 4), as both of them share grounding-independent mechanisms. In contrast, the grounded landfast ice (pink line, Fig. 4) shows a smooth, continuous increase with almost no short-term variability until the seasonal

https://doi.org/10.5194/egusphere-2026-826
Preprint. Discussion started: 20 May 2026

breakup, at which point it drops abruptly; its maximum extent occurs just before this breakup. Ungrounded fast ice generally forms earlier than grounded ice, which requires more time to accumulate because basal stress becomes effective only once the ice is sufficiently thick and grounded. Early in the landfast ice season, when ice is relatively thin, stabilization is provided mainly by local geometry.

The 3-year mean proportion of the grounded landfast ice to the total is about 56% for the entire Siberia Sea with significant regional variation. The East Siberia Sea has the highest proportion of 70%, followed by the Laptev Sea (about 54%) and the Kara Sea (41%) (Fig. 5). This suggests that a substantial fraction of the landfast ice in the Siberia Sea is stabilized by grounding-independent mechanisms.

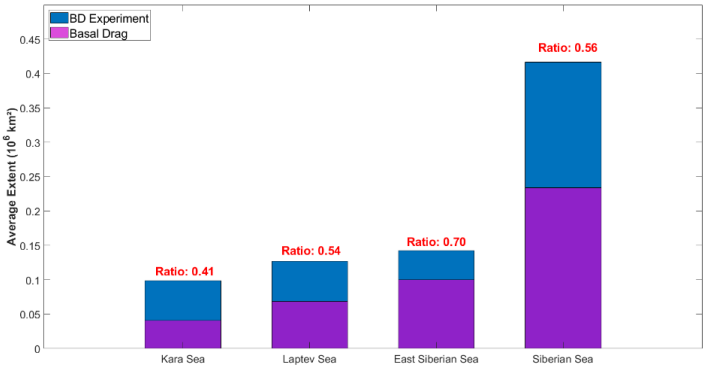

Figure 5: Contribution of grounded landfast ice to the total for the entire Siberia Sea and three individual seas.

3.3 Basal stress analysis

Figure 6 shows the occurrence of basal stress from January to May over the three-year period. The East Siberian Sea and Laptev Sea exhibit a high occurrence of basal stress, particularly near the New Siberian Islands. In contrast, within the Kara Sea, basal stress is confined predominantly to the estuaries of the Ob and Yenisei rivers. The spatial patterns of basal stress and landfast ice are similar in the Laptev and East Siberian Seas. However, in the Kara Sea, the extent of landfast is greater than the area of basal stress, because ice arcing is another important mechanism in the Kara Sea. Notably, basal stress not only generates landfast directly under grounded ice keels but also provides a stable platform for surrounding sea ice to attach, thereby facilitating a more extensive landfast ice cover. This mechanism allows the model to produce landfast ice over broader areas of shallow water.

https://doi.org/10.5194/egusphere-2026-826
Preprint. Discussion started: 20 May 2026

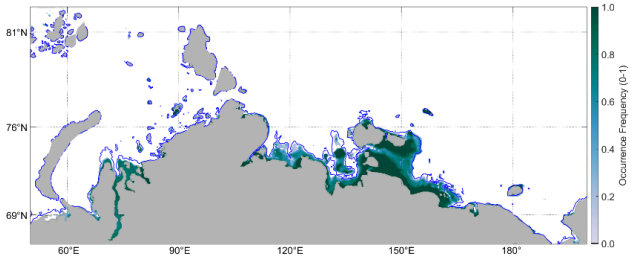

Figure 6: Occurrence of basal stress in the BD experiment from Jan to May over the 3-year period. The blue lines indicate the 20m bathymetric contour.

The averaged basal stress, wind stress and water stress over the grounded areas are shown in Fig.7. The basal and wind stresses act in opposite directions, and water stress is very small. During the freezing season, the magnitude of the basal stress is notably greater than that of both the wind stress and water stresses, with calculated values typically ranging from -0.2 to 0.2 N/m² and occasionally reaching -0.4 N/m². This substantial basal stress allows grounded ice to resist external forces and maintain stability. In contrast, the basal stress diminishes significantly during the melting season.

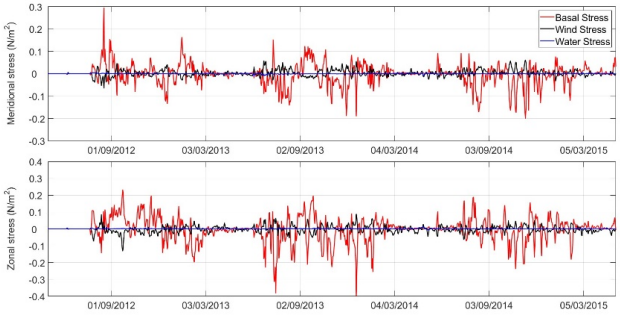

Figure 7: Time series of averaged basal stress (red line), water stress (blue line) and wind stress (black line) over the non-zero basal stress area in BD experiment from September 2012 to September 2015.

3.4 Midseason breakout events of the Landfast Ice

3.4.1 Identification of breakout events and offshore winds

Landfast ice generally remains stable through the freezing season due to high grounding stress, yet it remains susceptible to detachment during occasional strong winds. Here, a "breakout event" is defined by a rapid wintertime loss of at least 8% of landfast ice within one or two weeks. Based on this criterion, four breakout events were identified in the East Siberian Sea between 2012 and 2015 (Table 2). While the first event was resolved in bi-weekly data, the other three were identified at a weekly resolution. The corresponding BD simulation successfully captured all the four events, three of which occurred in April–May and one in January–February.

https://doi.org/10.5194/egusphere-2026-826
Preprint. Discussion started: 20 May 2026

Table 2: Midseason break out events in the East Siberian Sea

Event Number	Breakout date-NIC	Breakout date-BD	Pre-breakout total land fast ice area(km²)-BD	Breakout area (km²)-BD	Area of basal stress in breakout region (km²)-BD
1	04/22/2013-05/05/2013	04/21/2013-04/27/2013	3.77×10^5	0.83×10^5	0
2	04/10/2014-04/16/2014	04/10/2014-04/16/2014	3.78×10^5	1.18×10^5	76.67
3	01/29/2015-02/04/2015	01/30/2015-02/05/2015	2.52×10^5	0.64×10^5	40.37
4	05/07/2015-05/13/2015	05/10/2015-05/16/2015	3.08×10^5	0.28×10^5	4.04

Figure 8 illustrates that the four midseason breakouts all initiated along the outer edge of the landfast ice. The extents for the four breakouts, determined from the difference in landfast ice coverage between pre- and post-breakout, ranged from 0.28×10^5 km² to 1.18×10^5 km² (Table 2). This corresponds to 9-30% of the total landfast ice area prior to breakout. In all cases, the fractured ice displayed nearly zero basal stress, strongly suggesting that ungrounded landfast ice is significantly more vulnerable to breakouts than its grounded counterpart.

Similar to the studies from the Alaska coast (e.g. Jensen et al. 2023), the midseason breakout of landfast ice in the East Siberian Sea is also associated with offshore wind patterns. Figure 9 presents wind rose diagrams from the grid cells where breakout events occurred, comparing the 7-day event periods with the 12 days preceding and following them. The offshore southwesterly winds prevailed over the fractured area during the first three breakout events, and southwesterly prevailed during the fourth breakout event. The cumulative frequency of the prevailing wind direction exceeds 80% across all events, reaching over 95% in some cases. In contrast, winds during the pre- and post-event periods were more variable, with significantly low maximum frequencies smaller than 12%.

https://doi.org/10.5194/egusphere-2026-826
Preprint. Discussion started: 20 May 2026

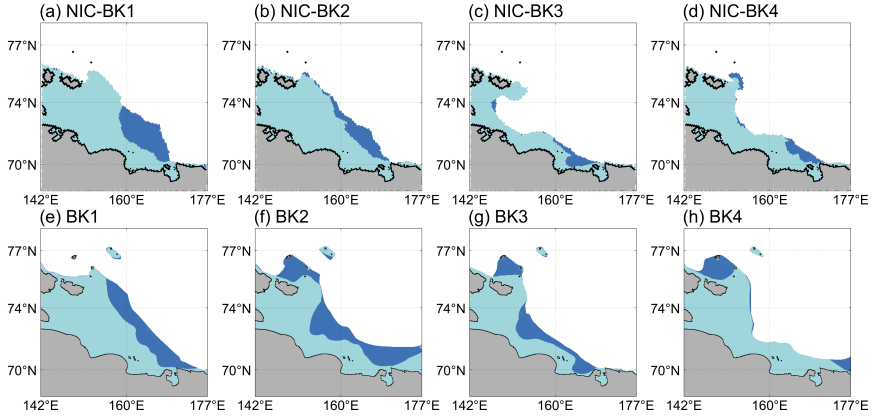

225 **Figure 8: Locations of the four breakout events in the East Siberian Sea. Light blue represents stable landfast ice, dark blue indicates the breakout areas. The top panels are derived from NIC ice charts, and the bottom subplots are from the BD experiment.**

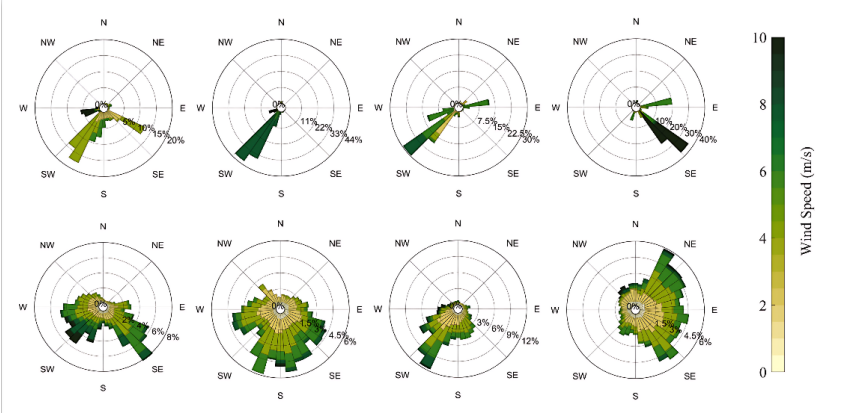

Figure 9: Wind rose plots for the breakout portion in the East Siberian Sea for the breakout events 1-4 (from left to right). The upper subplots are for 7-day breakout event periods, and the lower subplots are for 12 days pre- and post-events.

230 **3.4.2 Breakout events and cyclone passage**

Further analysis reveals that the four breakout events were driven by seven distinct cyclones traversing the East Siberian Sea. The trajectories of these cyclones (labeled sequentially 1-7) are shown in Figure 10. Figure 11 provides snapshots of the surface atmospheric conditions (sea level pressure, 2m temperature and 10m wind) at each cyclone's peak intensity, while Figure 12 details the daily ice detachment during the four breakout events. The spatial correspondence between the wind fields and the

235 location of detachment highlights the direct control of wind distribution on the breakout process.

https://doi.org/10.5194/egusphere-2026-826
Preprint. Discussion started: 20 May 2026

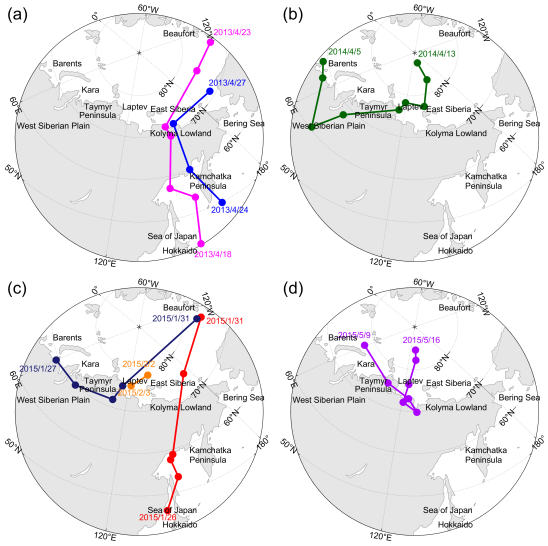

Figure 10 Daily trajectories of the cyclones linked to the four landfast ice breakout events, with panels (a) through (d) corresponding to events 1–4, respectively. These trajectories are derived from 6-hourly JRA-55 sea level pressure data. Unless otherwise indicated, the solid dots along each path mark the location of the cyclone center at 18:00 GMT each day.

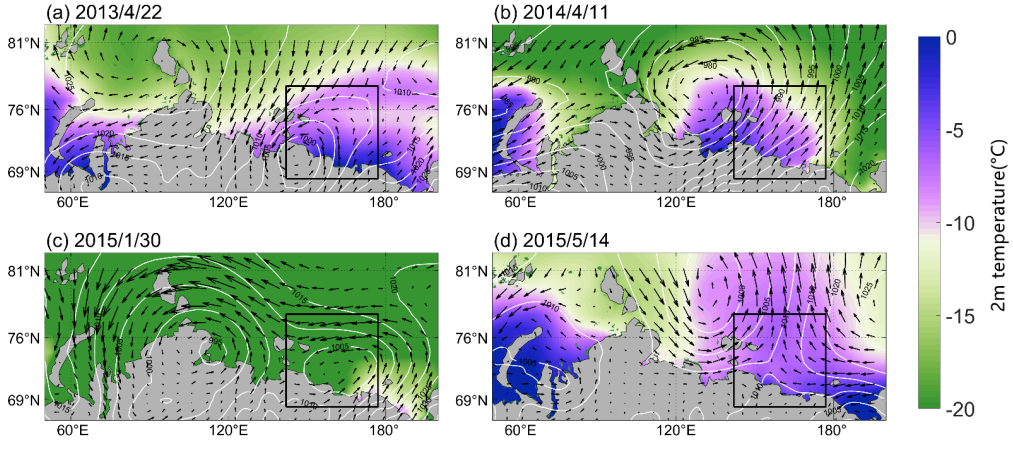

240

Figure 11 Snapshots of sea level pressure (white contours; 5 hPa interval), 10-m winds (vectors; m s^{-1}), and 2-m air temperature (shading; °C) for the storms that led to the four landfast ice breakout events.

https://doi.org/10.5194/egusphere-2026-826
Preprint. Discussion started: 20 May 2026

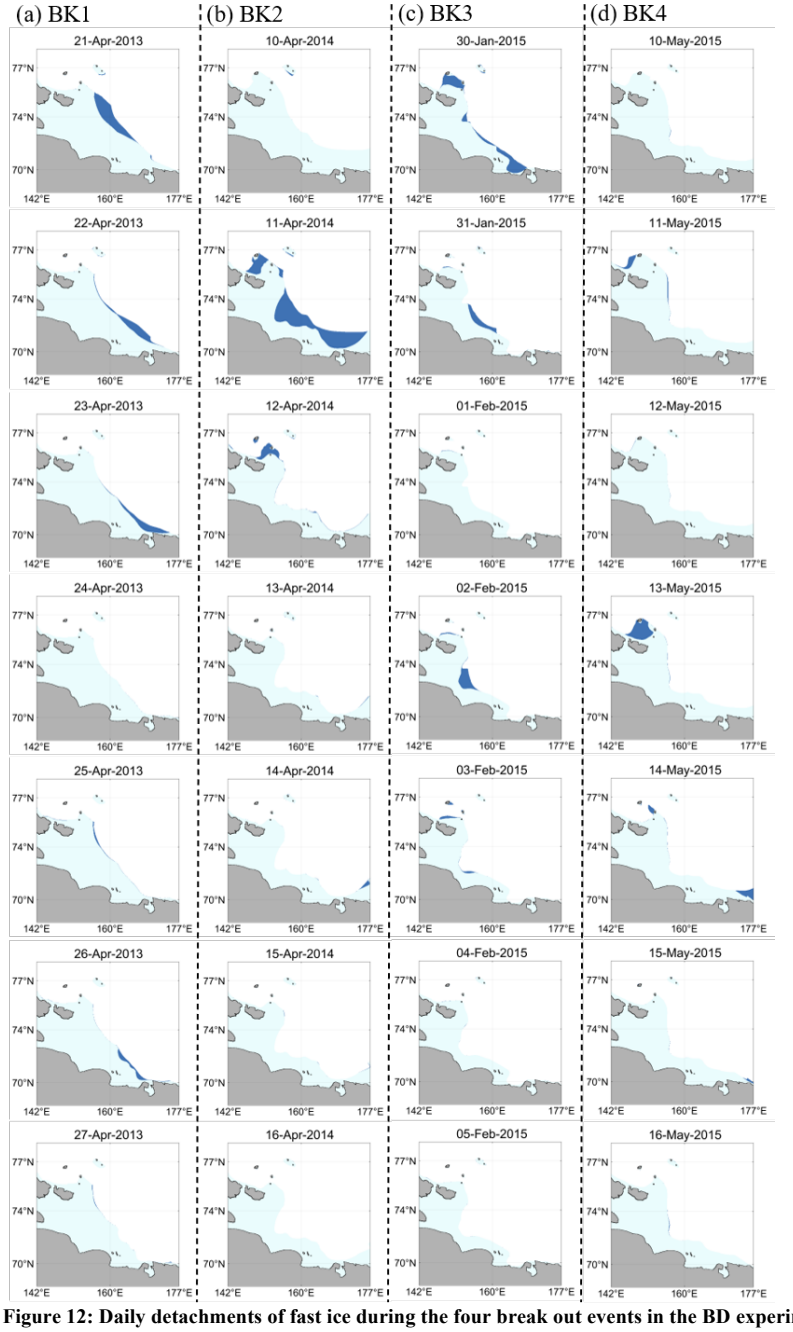

Figure 12: Daily detachments of fast ice during the four break out events in the BD experiment.

https://doi.org/10.5194/egusphere-2026-826
Preprint. Discussion started: 20 May 2026

The first breakout event (21–27 April 2013) was driven by two cyclones. Cyclone 1 developed east of Japan on 18 April, moving northward to the East Siberia Sea coast by 21-22 April. It induced warm air and southerly winds, destabilizing the fast ice along its outer edge and triggering an initial breakout in the northwest that extended southeastward. Cyclone 2, which formed south of the Kamchatka Peninsula on 24 April, reached the East Siberia Sea on 25 April. It generated strong westerly winds in the southeastern East Siberia Sea, causing a subsequent breakout in the southern part of the sea (Figs.10a,11a and 12a).

The second breakout Event occurred during 10–16 April 2014. Cyclone 3, originating over the southern Barents Sea on 5 April, tracked southeastward before being steered northeast by the Siberian high-pressure system. By 11 April, it had intensified into a large-scale sys Sea and western East Siberia Sea. The associated strong southerly and southwesterly winds caused substantial breakout along the northern, central, and eastern margins of the landfast ice. As the cyclone moved northward on 12 April, winds shifted to westerly, prompting further reduction of landfast ice northeast of the New Siberian Islands (Figures10b,11b and 12b).

The third breakout event occurred during 30 January–5 February 2015. Three cyclones (4-6) impacted the East Siberia Sea during this period. On 30 January, Cyclones 4 and 5 were positioned over the East Siberia Sea and Laptev Sea, respectively, while a weaker Cyclone 6 developed in the northwestern East Siberia Sea on 2-3 February. Cyclones 4 and 5 generated strong easterly (over the north) and westerly (over the south) winds, causing breakouts near the southern New Siberian Islands and western Ayon Island. A subsequent shift to southwesterly winds in the central and northern ESS triggered further breakout in the central region (Figures10c,11c and 12c).

The fourth breakout event occurred during 10–16 May 2015. This event was driven by Cyclone 7. Developing over the Barents Sea on 9 May, it travelled across the Taymyr Peninsula and lingered near the Laptev Sea coast. The cyclone's intensified southwesterly winds initially triggered a minor breakout in the northern East Siberia Sea. On 13 May, its interaction with the Beaufort High enhanced southerly winds over the northern Laptev and East Siberian Seas, leading to a major detachment of fast ice north of the New Siberian Islands (Figures10c,11c and 12c).

In summary, the four breakout events were consistently associated with the passage of cyclones that generated strong offshore winds, detaching landfast ice along its outer edge. During mid-season events, the cyclones' highest temperatures remained below the melting point, indicating that thermal forcing was negligible. Instead, these events were primarily driven by higher wind speeds compared to late-season breakups.

4 Discussion

In this study, we configured a high-resolution regional ocean-ice coupled model with a basal stress parameterization to simulate landfast ice and mid-season breakouts in the Siberian Seas. The model's fine grid accurately resolves coastal topography and islands, which is essential for realistic landfast ice simulation. It also incorporates climatological river runoff and a salinity-dependent freezing point. Leveraging these features, the model produces a realistic landfast ice distribution. Even without the

https://doi.org/10.5194/egusphere-2026-826
Preprint. Discussion started: 20 May 2026

grounding scheme, the control run of the high-resolution model reproduces approximately 44% of the observed landfast ice—significantly more than coarse-resolution models' standard runs (Lemieux et al., 2015, 2016; Liu et al., 2022). We have not incorporated the lateral drag parameterization proposed by Liu et al. (2022) in this simulation because the fine coastlines and small islands are already resolved in this high resolution model.

In the BD experiment, grounded ice constitutes approximately 56% of the total landfast ice area in the Siberian Seas. This proportion is even lower in the Kara Sea (41%), suggesting that a substantial fraction of the landfast ice is stabilized by geometric constraints. Further analysis indicts that the primary mechanism for landfast-ice formation appears to mostly depend on local geography. For example, the East Siberia Sea has the largest proportion of grounding ice (71%) and occurrence of basal stress (Fig. 6), while in the Laptev Sea, the proportion of grounding ice (54%) is slightly larger than the ungrounding ice (46%). This differences arises from the local topography. The topography in the East Siberia Sea is flatter than the Laptev Sea. The Laptev Sea features an intricate coastline and an uneven shelf with several valleys deeper than 20m (Fig. 1), thus the occurrence of basal stress in the Laptev Sea is much lower than the East Siberia Sea, because the grounding scheme mainly depends on the local water depth (Eq.1). Although the direct grounding ice constitutes approximately 54% of the total landfast ice in the Laptev Sea, basal stress in bulges may provide a stable platform for surrounding sea ice to attach, reproducing broader landfast ice coverage (Fig. 6). In addition, the coastline of the Laptev Sea is characterized by a shallow, highly indented mainland shore in the south featuring numerous bays and river deltas, and framed by major archipelagos to the west and east, which are favourable for the landfast ice to stabilize. Thus, the landfast ice in the Laptev Sea is quite stable with lower fluctuations than the East Siberia Sea and Kara Sea (Fig. 4).

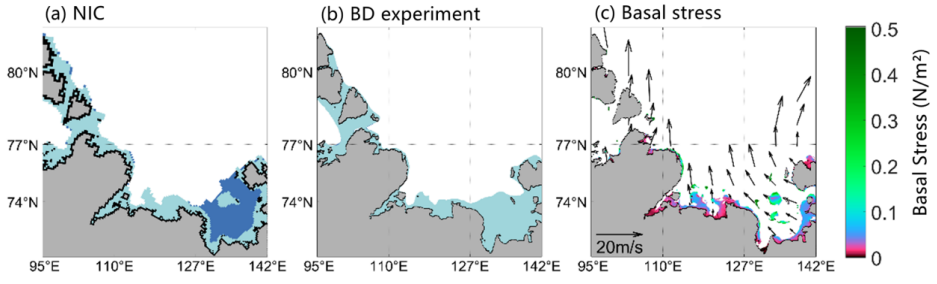

Figure 13: Landfast ice extent from the (a) NIC and (b) BD experiments for 6–13 February 2014. The breakout area is shown in dark blue, and stable ice is in light blue. (c) The corresponding basal stress magnitude (shaded, N m^{-2}) and 10 m wind velocity (vectors, m s^{-1}) on 13 February 2014. Only wind vectors with speeds below 10 m s^{-1} are displayed.

In the model the large basal stress in grounded ice typically allows it to resist strong winds during the freezing period while ungrounded ice is far more susceptible to fracture. This explains the four major midseason breakout events in the outer East Siberian Sea, where the landfast ice was both lacking in basal stress and geometric shelter. However, a prominent observed breakout event on 6-13 February 2014 in the southeastern Laptev Sea (Fig. 13a) was not found in the BD simulation. In the model, a large seabed elevation generates substantial basal stress (Fig. 13c). Both the observation and simulation show a

https://doi.org/10.5194/egusphere-2026-826
Preprint. Discussion started: 20 May 2026

stabilized landfast ice over this submarine bulge (Fig. 13a, c). The model did not reproduce the breakout occurring between the bulge and the surrounding shore despite strong southeasterly winds. This discrepancy may stem from the model parameters, like many other models, ours employs a high P-value (22460) to simulate landfast ice, which may increase ice strength and resistance to deformation.

The two free parameters in the basal stress scheme, k_1 and k_2, are tuned to simulate realistic landfast ice. As k_1 defines the critical mean thickness for activating basal stress (Eq. 1), it has the greatest impact (Lemieux et al., 2015). In this high-resolution model, a value of k_1=7 yielded more realistic simulations than k_1=8, which persistently overestimated the landfast ice extent. Figure 14 illustrates the magnitude and spatial distribution of basal stress on a typical day during each break out events for examples. In most cases, regions near the edges of the effective basal stress zone and some islands experience higher basal stress, while within the interior of the basal stress zone, basal stress remains lower, often below 0.2 N/m². However, on certain days, some areas exhibit exceptionally high basal stress, such as near the Delong Islands (Fig.14(d)). In areas where basal stress is in effect, the magnitude of basal stress is notably greater than that of sea ice-water stress and wind-ice stress (Fig.7). The comparatively large basal stress allows grounded ice to resist external forces and maintain stability in the majority of situations.

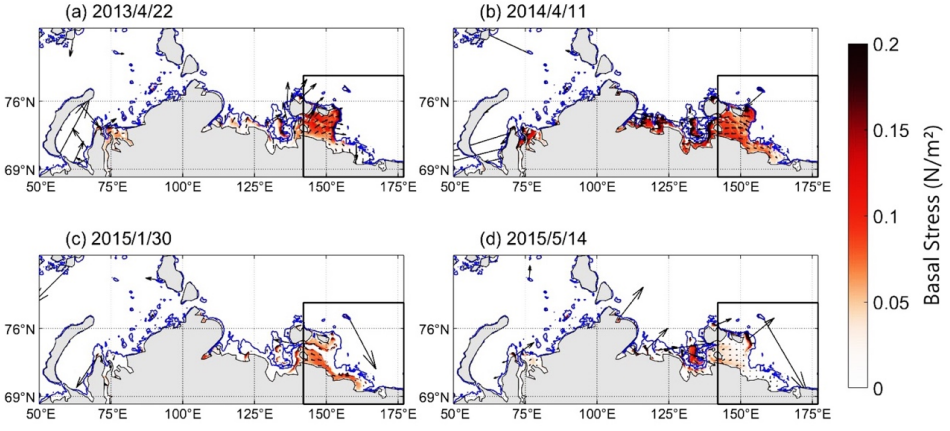

Figure 14: Basal stress calculated for typical days during the four landfast ice breakout events, with arrows showing stress direction.

5 Conclusion

A regional high resolution coupled sea ice-ocean model based on the MITgcm was set up to simulate landfast ice formation and midseason breakout on the Siberian shelf. As the fine grid well resolves the coastal topography and small islands, the high resolution model with the basal stress parameterization incorporated leads to a realistic landfast ice simulation in the Siberian Seas in terms of magnitude and seasonal cycle.

https://doi.org/10.5194/egusphere-2026-826
Preprint. Discussion started: 20 May 2026

The model results show that grounding mechanism accounts for approximately 56% of total landfast ice formation in the Siberia shelfs, and un-grounding processes also play vital roles. The contribution of the grounding mechanism varies regionally and depends strongly on local geography: the East Siberian Sea has the highest proportion of grounded ice (70%), followed by the Laptev Sea (54%) and the Kara Sea (41%).

The model successfully simulates midseason breakout events in the East Siberia Sea. These events all caused by the strong offshore winds and occured along the outer edge of the landfast ice, where basal stress was not active. Further anlaysis reveals that all the midseason breakout events were associated with the passage of cyclones, which induces the offshore winds fracturing the landfast ice into floating ice.

Code and Data availability

MITgcm code is available at https://github.com/MITgcm/MITgcm.The weekly/biweekly NIC Arctic Sea Ice Charts are available at https://nsidc.org/data/g10033/versions/1. The product of Estimating the Circulation and Climate of the Ocean, Phase II (ECCO2) is available at https://ecco-group.org/products.htm. Japanese 55-year Reanalysis (JRA-55) dataset can be found at https://gdex.ucar.edu/datasets/d628000/. Daily 4km Arctic Sea Ice Concentration is available at https://nsidc.org/data/g10005/versions/1. Extended AVHRR Polar Pathfinder (APP-X, Version 1) 12 hourly 25km sea ice thickness data are available at https://nsidc.org/data/nsidc-0746/versions/1. Polar Pathfinder Daily 25 km EASE-Grid Sea Ice Motion Vectors are from National Snow and Ice Data Center at https://nsidc.org/data/nsidc-0116/versions/4. Arctic River discharge and temperature (ARDAT) data set is available at http://research.cfos.uaf.edu/arctic-river/.

Author contributions

Conceptualization, XB and WZ; methodology, XB, KW, ZD and WZ; software: KW and ZD; Investigation: XB, KW and WZ, writing-original draft preparation XB and KW; writing—review and editing, XB, KW, XJ, and WZ; visualization, ZD and KW; supervision, XB; funding acquisition, XB. All authors have read and agreed to the published version of the manuscript.

Competing interests

The authors declare that they have no conflict of interest

https://doi.org/10.5194/egusphere-2026-826
Preprint. Discussion started: 20 May 2026

Disclaimer

Copernicus Publications remains neutral with regard to jurisdictional claims made in the text, published maps, institutional affiliations, or any other geographical representation in this paper. While Copernicus Publications makes every effort to include appropriate place names, the final responsibility lies with the authors. Views expressed in the text are those of the authors and do not necessarily reflect the views of the publisher.

Acknowledgements

The open-source datasets, including the Japan Reanalysis data, National Snow and Ice Data Centre (NSIDC) sea ice dataset, ECCO2 dataset, University of Alaska-Fairbanks (UAF) Arctic River discharge and temperature (ARDAT) data set are gratefully acknowledged.

Financial support

This research has been supported by the National Natural Science Foundation of China (grant no. 42276254).

References

Beatty, C. and Holland, D.: Modeling Landfast Sea Ice by Adding Tensile Strength, Journal of Physical Oceanography, 40, 185–198, https://doi.org/10.1175/2009JPO4105.1, 2010.

Bogardus, R., Maio, C., Mason, O., Buzard, R., Mahoney, A., and De Wit, C.: Mid-Winter Breakout of Landfast Sea Ice and Major Storm Leads to Significant Ice Push Event Along Chukchi Sea Coastline, Front. Earth Sci., 8, 344, https://doi.org/10.3389/feart.2020.00344, 2020.

Divine, D. V., Korsnes, R., and Makshtas, A. P.: Temporal and spatial variation of shore-fast ice in the Kara Sea, Continental Shelf Research, 24, 1717–1736, https://doi.org/10.1016/j.csr.2004.05.010, 2004.

Divine, D. V., Korsnes, R., Makshtas, A. P., Godtliebsen, F., and Svendsen, H.: Atmospheric- driven state transfer of shore-fast ice in the northeastern Kara Sea, J. Geophys. Res., 110, 2004JC002706, https://doi.org/10.1029/2004JC002706, 2005.

https://doi.org/10.5194/egusphere-2026-826
Preprint. Discussion started: 20 May 2026

Eicken, H., Dmitrenko, I., Tyshko, K., Darovskikh, A, Dierking, W., Blahak, U., Groves, J. and Kassens, H.: Zonation of the Laptev Sea land-fast ice cover and its importance in a frozen estuary, Global Planet. Change, 48, 55–83, https://doi:10.1016/j.gloplacha.2004.12.005, 2005.

Eicken, H., Lovecraft, A. L. and Druckenmiller, M. L.: Sea-ice system services: A framework to help identify and meet information needs relevant for Arctic observing networks, Arctic, 62, 119–136, 2009.

Fetterer, F., Stewart, J. S. & Meier, W. N.: MASAM2: Daily 4 km Arctic Sea Ice Concentration. (G10005, Version 1). [Data Set]. Boulder, Colorado USA. National Snow and Ice Data Center. https://doi.org/10.7265/N5ZS2TFT, 2015

Gearheard, S., Matumeak, W., Angutikjuaq, I., Maslanik, J., Huntington, H. P., Leavitt, J., Kagak, D. M., Tigullaraq, G., and Barry, R. G.: "It's Not that Simple": A Collaborative Comparison of Sea Ice Environments, Their Uses, Observed Changes, and Adaptations in Barrow, Alaska, USA, and Clyde River, Nunavut, Canada, AMBIO: A Journal of the Human Environment, 35, 203–211, https://doi.org/10.1579/0044-7447(2006)35%255B203:INTSAC%255D2.0.CO;2, 2006.

Haas, C., Dierking, W., Busche, T. and Hoelemann, J.: ENVISAT ASAR monitoring of polynya processes and sea ice production in the Laptev Sea, Proc. of the 2004 Envisat & ERS Symposium, Salzburg, Austria 6–10 September 2004, 2005

Hughes, N. E., Wilkinson, J. P., and Wadhams, P.: Multi-satellite sensor analysis of fast-ice development in the Norske Øer Ice Barrier, northeast Greenland, Ann. Glaciol., 52, 151–160, https://doi.org/10.3189/172756411795931633, 2011.

Hunke, E. C. and Dukowicz, J. K.: An Elastic–Viscous–Plastic Model for Sea Ice Dynamics, J. Phys. Oceanogr., 27, 1849–1867, https://doi.org/10.1175/1520-0485(1997)027%253C1849:AEVPMF%253E2.0.CO;2, 1997.

Itkin, P., Losch, M., and Gerdes, R.: Landfast ice affects the stability of the A rctic halocline: Evidence from a numerical model, JGR Oceans, 120, 2622–2635, https://doi.org/10.1002/2014JC010353, 2015.

Jakobsson, M., Mayer, L., Coakley, B., Dowdeswell, J. A., Forbes, S., Fridman, B., Hodnesdal, H., Noormets, R., Pedersen, R., Rebesco, M., Schenke, H. W., Zarayskaya, Y., Accettella, D., Armstrong, A., Anderson, R. M., Bienhoff, P., Camerlenghi, A., Church, I., Edwards, M., Gardner, J. V., Hall, J. K., Hell, B., Hestvik, O., Kristoffersen, Y., Marcussen, C., Mohammad, R., Mosher, D., Nghiem, S. V., Pedrosa, M. T., Travaglini, P. G., and Weatherall, P.: The International Bathymetric Chart of the Arctic Ocean (IBCAO) Version 3.0, Geophysical Research Letters, 39, 2012GL052219, https://doi.org/10.1029/2012GL052219, 2012.

Jensen, D. A., Nandan, V., Mahoney, A. R., Yackel, J. J., and Resler, L. M.: Landfast sea ice break out patterns in the northern Bering Sea observed from C-band Synthetic Aperture Radar, International Journal of Applied Earth Observation and Geoinformation, 117, 103183, https://doi.org/10.1016/j.jag.2023.103183, 2023.

Jones, J., Eicken, H., Mahoney, A., Mv, R., Kambhamettu, C., Fukamachi, Y., Ohshima, K. I., and George, J. C.: Landfast sea ice breakouts: Stabilizing ice features, oceanic and atmospheric forcing at Barrow, Alaska, Continental Shelf Research, 126, 50–63, https://doi.org/10.1016/j.csr.2016.07.015, 2016.

Key, J., Wang, X., Liu, Y., and NOAA CDR Program: NOAA Climate Data Record of AVHRR Polar Pathfinder Extended (APP-X), Version 2, NOAA National Centers for Environmental Information. doi:10.25921/AE96-0E57, 2019

https://doi.org/10.5194/egusphere-2026-826
Preprint. Discussion started: 20 May 2026

Kobayashi, S., Ota, Y., Harada, Y., Ebita, A., Moriya, M., Onoda, H., Onogi, K., Kamahori, H., Kobayashi, C., Endo, H., Miyaoka, K., and Takahashi, K.: The JRA-55 Reanalysis: General Specifications and Basic Characteristics, Journal of the Meteorological Society of Japan, 93, 5–48, https://doi.org/10.2151/jmsj.2015-001, 2015.

Lemieux, J., Dupont, F., Blain, P., Roy, F., Smith, G. C., and Flato, G. M.: Improving the simulation of landfast ice by combining tensile strength and a parameterization for grounded ridges, JGR Oceans, 121, 7354–7368, https://doi.org/10.1002/2016JC012006, 2016.

Lemieux, J., Lei, J., Dupont, F., Roy, F., Losch, M., Lique, C., and Laliberté, F.: The Impact of Tides on Simulated Landfast Ice in a Pan- Arctic Ice- Ocean Model, JGR Oceans, 123, 7747–7762, https://doi.org/10.1029/2018JC014080, 2018.

Lemieux, J., Tremblay, L. B., Dupont, F., Plante, M., Smith, G. C., and Dumont, D.: A basal stress parameterization for modeling landfast ice, JGR Oceans, 120, 3157–3173, https://doi.org/10.1002/2014JC010678, 2015.

Leng, H., Spall, M. A., Pickart, R. S., Lin, P., and Bai, X.: Origin and Fate of the Chukchi Slope Current Using a Numerical Model and In- Situ Data, JGR Oceans, 126, e2021JC017291, https://doi.org/10.1029/2021JC017291, 2021.

Liu, Y., Losch, M., Hutter, N., and Mu, L.: A New Parameterization of Coastal Drag to Simulate Landfast Ice in Deep Marginal Seas in the Arctic, JGR Oceans, 127, e2022JC018413, https://doi.org/10.1029/2022JC018413, 2022.

Losch, M., Menemenlis, D., Campin, J.-M., Heimbach, P., and Hill, C.: On the formulation of sea-ice models. Part 1: Effects of different solver implementations and parameterizations, Ocean Modelling, 33, 129–144, https://doi.org/10.1016/j.ocemod.2009.12.008, 2010.

Mahoney, A., Eicken, H., and Shapiro, L.: How fast is landfast sea ice? A study of the attachment and detachment of nearshore ice at Barrow, Alaska, Cold Regions Science and Technology, 47, 233–255, https://doi.org/10.1016/j.coldregions.2006.09.005, 2007a.

Mahoney, A., Eicken, H., Gaylord, A. G., and Shapiro, L.: Alaska landfast sea ice: Links with bathymetry and atmospheric circulation, J. Geophys. Res., 112, 2006JC003559, https://doi.org/10.1029/2006JC003559, 2007b.

Marshall, J., Hill, C., Perelman, L., and Adcroft, A.: Hydrostatic, quasi- hydrostatic, and nonhydrostatic ocean modeling, J. Geophys. Res., 102, 5733–5752, https://doi.org/10.1029/96JC02776, 1997.

Meier, W. N., Stroeve, J., and Gearheard, S.: Bridging perspectives from remote Sensing and Inuit communities on changing Sea-ice cover in the Baffin Bay region, Ann. Glaciol., 44, 433–438, https://doi.org/10.3189/172756406781811790, 2006.

Menemenlis, D., Campin, J.-M., Heimbach, P., Hill, C., Lee, T., Schodlok, M., and Zhang, H.: ECCO2: High Resolution Global Ocean and Sea Ice Data Synthesis, n.d.

Morales Maqueda, M. A., Willmott, A. J., and Biggs, N. R. T.: Polynya Dynamics: a Review of Observations and Modeling, Reviews of Geophysics, 42, 2002RG000116, https://doi.org/10.1029/2002RG000116, 2004.

Nguyen, A. T., Kwok, R., and Menemenlis, D.: Source and Pathway of the Western Arctic Upper Halocline in a Data-Constrained Coupled Ocean and Sea Ice Model, Journal of Physical Oceanography, 42, 802–823, https://doi.org/10.1175/JPO-D-11-040.1, 2012.

https://doi.org/10.5194/egusphere-2026-826
Preprint. Discussion started: 20 May 2026

Olason, E.: A dynamical model of Kara Sea land- fast ice, JGR-Oceans, 121, 3141–3158, https://doi.org/10.1002/2016JC011638, 2016.

Radosavljevic, B., Lantuit, H., Pollard, W., Overduin, P., Couture, N., Sachs, T., Helm, V., and Fritz, M.: Erosion and Flooding—Threats to Coastal Infrastructure in the Arctic: A Case Study from Herschel Island, Yukon Territory, Canada, Estuaries and Coasts, 39, 900–915, https://doi.org/10.1007/s12237-015-0046-0, 2016.

Selyuzhenok, V., Krumpen, T., Mahoney, A., Janout, M., and Gerdes, R.: Seasonal and interannual variability of fast ice extent in the southeastern L aptev S ea between 1999 and 2013, JGR Oceans, 120, 7791–7806, https://doi.org/10.1002/2015JC011135, 2015.

Selyuzhenok, V., Mahoney, A., Krumpen, T., Castellani, G., and Gerdes, R.: Mechanisms of fast-ice development in the south-eastern Laptev Sea: a case study for winter of 2007/08 and 2009/10, Polar Research, 36, 1411140, https://doi.org/10.1080/17518369.2017.1411140, 2017.

Tremblay, L.-B. and Hakakian, M.: Estimating the Sea Ice Compressive Strength from Satellite-Derived Sea Ice Drift and NCEP Reanalysis Data*, Journal of Physical Oceanography, 36, 2165–2172, https://doi.org/10.1175/JPO2954.1, 2006.

Tschudi, M., Meier, W. N., Stewart, J. S., Fowler, C. & Maslanik, J.: Polar Pathfinder Daily 25 km EASE-Grid Sea Ice Motion Vectors. (NSIDC-0116, Version 4). [Data Set]. Boulder, Colorado USA. NASA National Snow and Ice Data Center Distributed Active Archive Center. https://doi.org/10.5067/INAWUWO7QH7B, 2019

Whitefield, J., Winsor, P., McClelland, J., and Menemenlis, D.: A new river discharge and river temperature climatology data set for the pan-Arctic region, Ocean Modelling, 88, 1–15, https://doi.org/10.1016/j.ocemod.2014.12.012, 2015.

Yu, Y., Stern, H., Fowler, C., Fetterer, F., and Maslanik, J.: Interannual Variability of Arctic Landfast Ice between 1976 and 2007, Journal of Climate, 27, 227–243, https://doi.org/10.1175/JCLI-D-13-00178.1, 2014.

Zhai, M., Leppäranta, M., Cheng, B., Lei , R., and Zhang, F., Physics of arctic landfast sea ice and implications on the cryosphere : An overview, Advances in Polar Science, 32 (4), 278-291 . https://doi.org/10.13679/j.advps.2021.0040, 2021

Zhang, J. and Hibler, W. D.: On an efficient numerical method for modeling sea ice dynamics, J. Geophys. Res., 102, 8691–8702, https://doi.org/10.1029/96JC03744, 1997.